

Adaptive fast multipole boundary element method for three-dimensional half-space acoustic wave problems

M.S. Bapat, L. Shen, Y.J. Liu *

Computer-Aided Engineering Research Laboratory, Department of Mechanical Engineering, University of Cincinnati, Cincinnati, OH 45221-0072, USA

ARTICLE INFO

Article history:

Received 26 March 2008

Accepted 9 April 2009

Available online 15 May 2009

Keywords:

Acoustics

3D half space

Fast multipole BEM

Windmill models

ABSTRACT

A new adaptive fast multipole boundary element method (BEM) for solving 3-D half-space acoustic wave problems is presented in this paper. The half-space Green's function is employed explicitly in the boundary integral equation (BIE) formulation so that a tree structure of the boundary elements only for the boundaries of the real domain need to be applied, instead of using a tree structure that contains both the real domain and its mirror image. This procedure simplifies the implementation of the adaptive fast multipole BEM and reduces the CPU time and memory storage by about a half for large-scale half-space problems. An improved adaptive fast multipole BEM is presented for the half-space acoustic wave problems, based on the one developed recently for the full-space problems. This new fast multipole BEM is validated using several simple half-space models first, and then applied to model 3-D sound barriers and a large-scale windmill model with five turbines. The largest BEM model with 557470 elements was solved in about an hour on a desktop PC. The accuracy and efficiency of the BEM results clearly show the potential of the adaptive fast multipole BEM for solving large-scale half-space acoustic wave problems that are of practical significance.

© 2009 Elsevier Ltd. All rights reserved.

1. Introduction

The boundary element method (BEM) is an efficient tool for solving exterior acoustic wave problems due to its features of boundary discretization and automatic satisfaction of the Sommerfeld radiation condition at infinity. When dealing with half-space problems, the so called half-space Green's function [1] can be applied by adding the source solution at the image point to the original full-space Green's function. Using this half-space Green's function, the discretization of the rigid infinite plane is removed and only the boundaries of the structure need to be discretized. All these advantages make the BEM an attractive candidate for analyzing half-space acoustic problems.

The reduction of operation counts for the BEM has been achieved by adopting the fast multipole method (FMM) [2,3] to perform the matrix–vector multiplication with an iterative solver (e.g., GMRES). Many fast multipole BEM (FMBEM) approaches for modeling acoustic problems in the infinite domain have been reported in the literature (see Refs. [4–10], a review in [11] and a book in [12]). Although the FMM algorithm for full-space Helmholtz equation has been covered extensively in the literature,

the application of the FMBEM to 3-D half-space wave problems is relatively new.

The FMBEM for full-space acoustic problems can be applied in solving the half-space problems by simply using the mirror image technique. However, this approach comes with a penalty. When using the FMBEM to solve a full-space problem, a hierarchical tree of boxes is used to group all elements on the structure. While in solving a half-space problem using the full-space FMBEM, both the structure above the infinite plane and its mirror image below the infinite plane need to be discretized. Therefore, a larger hierarchical tree of boxes is required to group all nodes and their mirror image points in a naïve manner. The situation becomes worse as the distance between the structure and the infinite plane increases, leading to an even larger tree structure. This deficiency in using the full-space FMBEM for solving half-space problems has been shown in Ref. [13] and will be demonstrated again in this paper.

In Ref. [13], Yasuda and Sakuma proposed an efficient technique for solving 3-D sound field with plane symmetry using the fast multipole BEM. In their approach to plane symmetry problems, the half-space Green's function is not employed in the boundary integral equation (BIE) formulation explicitly. Instead, the original full-space Green's function is used in the BIE and the full-space BEM is applied to the real domain and its mirror image domain. The relations among the matrices due to the symmetry of the BEM models are employed to save the computations. Their

* Corresponding author. Tel.: +1513 556 4607; fax: +1513 556 3390.
E-mail address: Yijun.Liu@uc.edu (Y.J. Liu).

method is applicable to problems that have one, two, or three symmetrical planes, and is therefore not limited to half-space problems. Using this method, the CPU time and memory size can be cut in half for problems with one symmetry plane. The largest symmetrical BEM model solved in Ref. [13] has 49152 DOFs (degrees of freedom) for an interior domain with one symmetry plane.

In the present study, the adaptive FMBEM approach of Cheng et al. [14] and Shen and Liu [10,15] is extended to solve half-space acoustic wave problems, in which only the elements Green's function is applied explicitly in the BIE formulation for half-space acoustic problems. Using the half-space Green's function, the implementation of half-space FMBEM is simplified, where only the local expansion is different from that for the full-space FMBEM. The total CPU time and memory storage are also reduced by about a half for large half-space BEM models, the same as concluded in Ref. [13] based on utilizing the symmetry features of the discretized BEM equations. Large half-space acoustic BEM models with the number of DOFs equal to 557470 are solved with the developed FMBEM on a PC in about an hour with the tolerance for convergence set at 10^{-5} using the GMRES solver. This clearly demonstrates the efficiency and potential of the developed fast multipole BEM for solving large-scale half-space acoustic problems.

The paper is organized as follows: Section 2 reviews the basic FMBEM formulation for half-space problems. Section 3 introduces the adaptive FMBEM algorithm, where the same hierarchical tree used in the full-space domain is used. Section 4 shows the numerical results and comparisons between the half-space and full-space FMBEM. Discussions on further improvement of the method are presented in Section 5 to conclude the paper.

2. Formulation of the FMBEM for half-space acoustic problems

The direct boundary integral equation for the Helmholtz equation which governs the acoustic wave problems can be written as

$$c(\mathbf{x})\varphi(\mathbf{x}) = \int_{\Gamma} [G(\mathbf{x}, \mathbf{y})q(\mathbf{y}) - F(\mathbf{x}, \mathbf{y})\varphi(\mathbf{y})] d\Gamma(\mathbf{y}) + \varphi^l(\mathbf{x}) \quad \forall \mathbf{x} \in \Gamma, \quad (1)$$

where φ is the acoustic pressure, $q = \partial\varphi/\partial n$, φ^l represents a typical incident wave (which should satisfy the half-space condition), n the outward normal, and the coefficient c is $\frac{1}{2}$ if the surface Γ is smooth around source point \mathbf{x} . For half-space problems with a rigid infinite symmetry plane (where the velocity is zero), the Green's function is [1]

$$G(\mathbf{x}, \mathbf{y}) \equiv G(\mathbf{x}, \mathbf{x}', \mathbf{y}) = \frac{e^{ik|\mathbf{x}-\mathbf{y}|}}{4\pi|\mathbf{x}-\mathbf{y}|} + \frac{e^{ik|\mathbf{x}'-\mathbf{y}|}}{4\pi|\mathbf{x}'-\mathbf{y}|}, \quad (2)$$

where \mathbf{x}' is the mirror image point of the source point \mathbf{x} (Fig. 1), \mathbf{y} the field point, k the wavenumber and $i = \sqrt{-1}$. For a soft infinite symmetry plane (where the pressure is zero), the plus sign in the above expression should be changed to a minus sign.

The boundary conditions are:

$$\begin{cases} \varphi(\mathbf{x}) = \bar{\varphi}(\mathbf{x}), & \forall \mathbf{x} \in \Gamma_1, \\ q(\mathbf{x}) = \bar{q}(\mathbf{x}), & \forall \mathbf{x} \in \Gamma_2, \end{cases} \quad (3)$$

where $\Gamma = \Gamma_1 \cup \Gamma_2$, and the barred quantities indicate given values on the boundary.

Discretizing the boundary Γ using N (e.g., constant) surface elements leads to the following system of equations (e.g., for

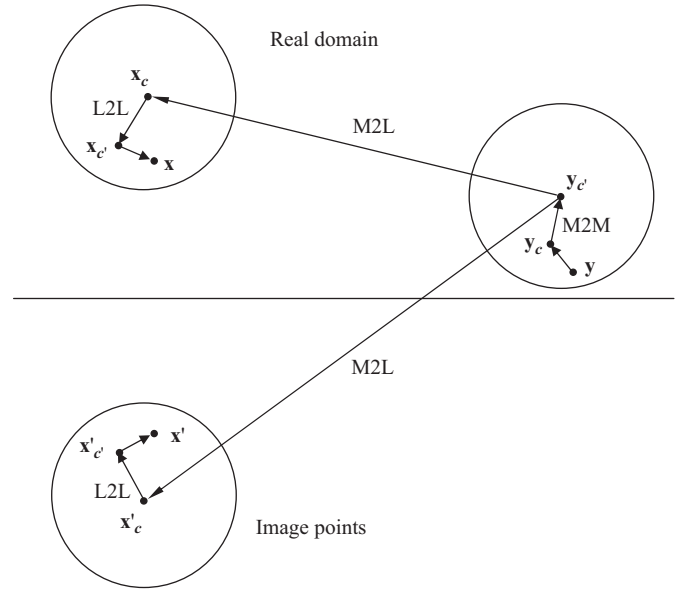


Fig. 1. M2M, M2L, L2L translation in half-space.

radiation problems):

$$\sum_{j=1}^N f_{ij}\varphi_j = \sum_{j=1}^N g_{ij}q_j \quad \text{for node } i = 1, 2, \dots, N, \quad (4)$$

where

$$g_{ij} = \int_{\Delta\Gamma_j} G(\mathbf{x}_i, \mathbf{x}', \mathbf{y}) d\Gamma(\mathbf{y}) \quad f_{ij} = \int_{\Delta\Gamma_j} F(\mathbf{x}_i, \mathbf{x}', \mathbf{y}) d\Gamma(\mathbf{y}) + \frac{1}{2}\delta_{ij}, \quad (5)$$

in which $\Delta\Gamma_j$ represents element j (in the case of using constant elements).

Re-arranging each term in Eq. (4), that is, moving the unknown terms to the left-hand side and known terms to the right-hand side, we can write Eq. (4) as

$$\begin{bmatrix} a_{11} & a_{12} & \dots & a_{1N} \\ a_{21} & a_{22} & \dots & a_{2N} \\ \vdots & \vdots & \ddots & \vdots \\ a_{N1} & a_{N2} & \dots & a_{NN} \end{bmatrix} \begin{Bmatrix} \lambda_1 \\ \lambda_2 \\ \vdots \\ \lambda_N \end{Bmatrix} = \begin{Bmatrix} b_1 \\ b_2 \\ \vdots \\ b_N \end{Bmatrix}, \quad \text{or } \mathbf{A}\boldsymbol{\lambda} = \mathbf{b}, \quad (6)$$

where \mathbf{A} is the system matrix, $\boldsymbol{\lambda}$ the unknown vector, \mathbf{b} the product of known boundary value vector and corresponding coefficient matrix.

To solve Eq. (6) using iterative solver, $\mathbf{A}\boldsymbol{\lambda}$ is calculated in each iteration step. Conventional way to calculate the $\mathbf{A}\boldsymbol{\lambda}$ takes $O(N^2)$ operation count, as well as $O(N^2)$ memory storage. Using the FMM will reduce the operation count from $O(N^2)$ to $O(N)$, and memory size from $O(N^2)$ to $O(N)$. In the following, the basic FMM formulas for the Helmholtz equation are reviewed.

As depicted in Fig. 1, the fundamental solution of the half-space Green's function G represents the interaction between the source point \mathbf{x} and field point \mathbf{y} , and the interaction between mirror point \mathbf{x}' and field point \mathbf{y} . It can be expressed as a multipole expansion

$$G = \frac{ik}{4\pi} \sum_{n=0}^{\infty} (2n+1) \sum_{m=-n}^n \bar{I}_n^m(k, \mathbf{y}, \mathbf{y}_c) [O_n^m(k, \mathbf{x}, \mathbf{y}_c) + O_n^m(k, \mathbf{x}', \mathbf{y}_c)], \quad |\mathbf{y} - \mathbf{y}_c| < |\mathbf{x} - \mathbf{y}_c|, \quad (7)$$

where the inner function I_n^m is in the form

$$I_n^m(k, \mathbf{y}, \mathbf{y}_c) = j_n(k|\mathbf{y} - \mathbf{y}_c|) Y_n^m \left(\frac{\mathbf{y} - \mathbf{y}_c}{|\mathbf{y} - \mathbf{y}_c|} \right), \quad (8)$$

the outer function O_n^m is defined by

$$O_n^m(k, \mathbf{x}, \mathbf{y}_c) = h_n^{(1)}(k|\mathbf{x} - \mathbf{y}_c|)Y_n^m\left(\frac{\mathbf{x} - \mathbf{y}_c}{|\mathbf{x} - \mathbf{y}_c|}\right), \quad (9)$$

and j_n is the spherical Bessel function, $h_n^{(1)}$ the spherical Hankel function of the first kind and Y_n^m the spherical harmonics [16].

For integrals on element j which is far away from the source point \mathbf{x} ($|\mathbf{y} - \mathbf{y}_c| < |\mathbf{x} - \mathbf{y}_c|$), the integrations in Eq. (5) can then be written as the multipole expansions around \mathbf{y}_c as follows:

$$\begin{aligned} & \int_{\Delta\Gamma_j} G(\mathbf{x}_i, \mathbf{x}'_i, \mathbf{y})q_j d\Gamma(\mathbf{y}) \\ &= \frac{ik}{4\pi} \sum_{n=0}^{\infty} (2n+1) \sum_{m=-n}^n M_{nj}^m(k, \mathbf{y}_c) [O_n^m(k, \mathbf{x}_i, \mathbf{y}_c) + O_n^m(k, \mathbf{x}'_i, \mathbf{y}_c)], \\ & \int_{\Delta\Gamma_j} \frac{\partial G(\mathbf{x}_i, \mathbf{x}'_i, \mathbf{y})}{\partial n(\mathbf{y})} \varphi_j d\Gamma(\mathbf{y}) \\ &= \frac{ik}{4\pi} \sum_{n=0}^{\infty} (2n+1) \sum_{m=-n}^n \tilde{M}_{nj}^m(k, \mathbf{y}_c) [O_n^m(k, \mathbf{x}_i, \mathbf{y}_c) + O_n^m(k, \mathbf{x}'_i, \mathbf{y}_c)], \end{aligned} \quad (10)$$

where the multipole moments are defined as

$$\begin{aligned} M_{nj}^m(k, \mathbf{y}_c) &= \int_{\Delta\Gamma_j} \tilde{I}_n^m(k, \mathbf{y}, \mathbf{y}_c)q_j d\Gamma(\mathbf{y}), \\ \tilde{M}_{nj}^m(k, \mathbf{y}_c) &= \int_{\Delta\Gamma_j} \frac{\tilde{I}_n^m(k, \mathbf{y}, \mathbf{y}_c)}{\partial n(\mathbf{y})} \varphi_j d\Gamma(\mathbf{y}). \end{aligned} \quad (11)$$

Information of a group of element Γ_j that are close to \mathbf{y}_c can be added up and stored in one set of multipole moments $M_n^m(k, \mathbf{y}_c)$ given by

$$M_n^m(k, \mathbf{y}_c) = \sum_j M_{nj}^m(k, \mathbf{y}_c), \quad (12)$$

where j is the number of an element.

The multipole moment center can be moved from \mathbf{y}_c to \mathbf{y}_c' using the moment-to-moment (M2M) translation, if $|\mathbf{y} - \mathbf{y}_c| < |\mathbf{x} - \mathbf{y}_c|$

$$\begin{aligned} M_n^m(k, \mathbf{y}_c) &= \sum_{n'=0}^{\infty} \sum_{m'=-n'}^{n'} \sum_{\substack{l=|n-n'| \\ n+n'-l \text{ even}}}^{n+n'} (2n'+1)(-1)^m W_{n,n',m,m',l} \tilde{I}_l^{m-m'}(k, \mathbf{y}_c, \mathbf{y}_c') \\ &\quad \times M_{n'}^{m'}(k, \mathbf{y}_c), \end{aligned} \quad (13)$$

where $W_{n,n',m,m',l}$ is calculated using the following formula:

$$W_{n,n',m,m',l} = (2l+1)i^{n'-n+l} \begin{pmatrix} n & n' & l \\ 0 & 0 & 0 \end{pmatrix} \begin{pmatrix} n & n' & l \\ m & m' & -m-m' \end{pmatrix},$$

and $\begin{pmatrix} * & * & * \\ * & * & * \end{pmatrix}$ denotes the Wigner 3j symbol.

The expansion center can also be moved from \mathbf{y}_c to \mathbf{x}_c through multipole-to-local translation (M2L), given $|\mathbf{x} - \mathbf{x}_c| < |\mathbf{y} - \mathbf{x}_c|$ and $|\mathbf{y} - \mathbf{y}_c| < |\mathbf{x} - \mathbf{y}_c|$. The resulting expansion is called local expansion and the local expansion coefficients $L_n^m(k, \mathbf{x}_c)$ can be expressed as

$$\begin{aligned} L_n^m(k, \mathbf{x}_c) &= \sum_{n'=0}^{\infty} \sum_{m'=-n'}^{n'} \sum_{\substack{l=|n-n'| \\ n+n'-l \text{ even}}}^{n+n'} (2n'+1)W_{n',n,m',m,l} \tilde{O}_l^{m-m'} \\ &\quad \times (k, \mathbf{x}_c, \mathbf{y}_c)M_{n'}^{m'}(k, \mathbf{y}_c), \end{aligned} \quad (14)$$

where $\tilde{O}_l^m(k, \mathbf{x}, \mathbf{y}) = h_n^{(1)}(k|\mathbf{x} - \mathbf{y}|)\tilde{Y}_n^m(\mathbf{x} - \mathbf{y})$. Similarly, moving the multipole expansion center from \mathbf{y}_c to \mathbf{x}'_c , which is the mirror image point of \mathbf{x}_c , will have another set of local expansion coefficients

$$\begin{aligned} L_n^m(k, \mathbf{x}'_c) &= \sum_{n'=0}^{\infty} \sum_{m'=-n'}^{n'} \sum_{\substack{l=|n-n'| \\ n+n'-l \text{ even}}}^{n+n'} (2n'+1)W_{n',n,m',m,l} \tilde{O}_l^{m-m'} \\ &\quad \times (k, \mathbf{x}'_c, \mathbf{y}_c)M_{n'}^{m'}(k, \mathbf{y}_c). \end{aligned} \quad (15)$$

The local expansion center \mathbf{x}_c (\mathbf{x}'_c) can be moved to \mathbf{x}_c' (\mathbf{x}'_c') using local-to-local translation (L2L), given $|\mathbf{x} - \mathbf{x}_c| < |\mathbf{y} - \mathbf{x}_c|$

$$\begin{aligned} L_n^m(k, \mathbf{x}_c) &= \sum_{n'=0}^{\infty} \sum_{m'=-n'}^{n'} \sum_{\substack{l=|n-n'| \\ n+n'-l \text{ even}}}^{n+n'} (2n'+1)(-1)^m W_{n',n,m',-m,l} \tilde{I}_l^{m-m'} \\ &\quad \times (k, \mathbf{x}_c', \mathbf{x}_c) L_{n'}^{m'}(k, \mathbf{x}_c), \\ L_n^m(k, \mathbf{x}'_c) &= \sum_{n'=0}^{\infty} \sum_{m'=-n'}^{n'} \sum_{\substack{l=|n-n'| \\ n+n'-l \text{ even}}}^{n+n'} (2n'+1)(-1)^m W_{n',n,m',-m,l} \tilde{I}_l^{m-m'} \\ &\quad \times (k, \mathbf{x}'_c', \mathbf{x}'_c) L_{n'}^{m'}(k, \mathbf{x}'_c). \end{aligned} \quad (16)$$

M2M, M2L, L2L translations are depicted in Fig. 1.

Finally, for a group of field points \mathbf{y}_j that are far away from the source point \mathbf{x}_i , $g_{ij}q_j$ or $f_{ij}\varphi_j$ can be expressed by the following local expansion in terms of the local coefficients which are functions of \mathbf{x}_c , \mathbf{x}'_c , \mathbf{x}_i , \mathbf{x}'_i and k :

$$\begin{aligned} g_{ij}q_j \text{ or } f_{ij}\varphi_j &= \frac{ik}{4\pi} \sum_{n=0}^{\infty} (2n+1) \sum_{m=-n}^n [L_n^m(k, \mathbf{x}_c) \tilde{I}_n^m(k, \mathbf{x}_i, \mathbf{x}_c) \\ &\quad + L_n^m(k, \mathbf{x}'_c) \tilde{I}_n^m(k, \mathbf{x}'_i, \mathbf{x}'_c)]. \end{aligned} \quad (17)$$

From the above equation, we can see that there are two sets of local coefficients. $L_n^m(k, \mathbf{x}_c)$ is for the real domain and $L_n^m(k, \mathbf{x}'_c)$ for the image domain. However, it is unnecessary to create a hierarchical tree of boxes to include the image domain, since \mathbf{x}'_c is dependent on the location of \mathbf{x}_c and the rigid infinite plane. For elements that are close to the source point \mathbf{x}_i , the conventional direct evaluation of the integrals (Eq. (5)) is used.

To determine the number (p) of terms in the multipole and local expansions, the following empirical formula (see, Ref. [11]) is applied:

$$p = kD + c_0 \log(kD + \pi), \quad (18)$$

where D is the diameter of the cell on which expansions are calculated, and c_0 a number depending on the precision of the arithmetic. Formula (18) can be applied to adaptively determine the values of p at different tree levels in the fast multipole algorithms.

The fast multipole formulations discussed above for solving 3-D acoustic wave problems or Helmholtz equation in general are good for low frequencies, because of the $O(p^5)$ nature of the formulation. To perform the M2M, M2L and L2L translations, $O(p^5)$ computations are required since there are three summations in all these translations and two indices in the coefficients, as shown in Eqs. (13)–(16). In addition, the use of the Wigner-3j symbol in Eqs. (13)–(16), which is time consuming to calculate each time and consumes more memory if its values are stored, further reduces the computational efficiency.

Theorems have been set up by Gumerov in Ref. [17] for recurrence relations for the calculation of expansion coefficients that can reduce the complexity for the translations to $O(p^4)$. Chew also summarized these theorems earlier in Ref. [18].

For example, the M2L translation in Eq. (14) can be expressed in operator terms as

$$L_n^m(k, \mathbf{x}_c) = M|L_{n,n'}^{m,m'}(k, \mathbf{x}_c, \mathbf{y}_c)M_{n'}^{m'}(k, \mathbf{y}_c), \quad (19)$$

where the M2L operator $M|L$ is given by

$$M|L_{n,n'}^{m,m'}(k, \mathbf{x}_c, \mathbf{y}_c) = \sum_{\substack{l=|n-n'| \\ n+n'-l \text{ even}}}^{n+n'} (2n'+1)W_{n',n,m',m,l} \tilde{O}_l^{m-m'}(k, \mathbf{x}_c, \mathbf{y}_c). \quad (20)$$

The method relies on explicitly finding the operators $M|L_{0,n}^{0,m}(k, \mathbf{x}_c, \mathbf{y}_c)$ and $M|L_{n,0}^{0,0}(k, \mathbf{x}_c, \mathbf{y}_c)$ from the definition. These ‘‘Sectorial’’ operators start the initialization point for the recursive scheme. The generalized operators are then evaluated using the recursive formulas given by

$$b_{m+1}^{-(m+1)} M|L_{s,m+1}^{t,m+1} = b_s^{-t} M|L_{s-1,m}^{t-1,m} + b_{s+1}^{t-1} M|L_{s+1,m}^{t-1,m}, \quad (21)$$

$$b_{m+1}^{-(m+1)} M|L_{s,m+1}^{t, -(m+1)} = b_s^t M|L_{s-1,m}^{t+1, -m} + b_{s+1}^{-(t+1)} M|L_{s+1,m}^{t+1, -m}, \quad (22)$$

$$a_n^m M|L_{s,n+1}^{t,m} = a_{n-1}^m M|L_{s,n-1}^{t,m} - a_s^t M|L_{s+1,n}^{t,m} + a_{s-1}^t M|L_{s-1,n}^{t,m}. \quad (23)$$

The constants a_n^m and b_n^m in the above equations depend on the choice of the spherical harmonics. Similar approaches can be followed for the M2M and L2L translations.

Ong et al. have used this $O(p^4)$ scheme to calculate fast Fourier transforms [19]. Although the number of operations can be reduced to $O(p^4)$ by employing the above recursive relations, the computing time can still increase quickly with the increase in the value of p .

For higher frequency problems, the diagonal form proposed by Rokhlin [20] can be employed to accelerate the computations of all the translations. Unfortunately, this diagonal form breaks down at lower frequencies, where the original formulations will need to be applied [11]. The wideband fast multipole method proposed by Cheng et al. [21] may be considered, which provides a seamless framework for combining the low and high frequency formulations.

In this study, the $O(p^3)$ formulation developed by Gumerov and Duraiswami [22,23] that uses special co-ordinate transformations in addition to the recursive $O(p^4)$ scheme has been implemented. The $M|L$ operator in Eq. (20) reduces to zero under certain conditions based on the orientation of the vector $\mathbf{x}_c - \mathbf{y}_c$. Only the operator $M|L_{n,n'}^m = M|L_{n,n'}^{m,-m}(k, \mathbf{x}_c, \mathbf{y}_c)$ needs to be calculated in this case because the other terms are zero. The non-zero $M|L$ operator ($M|L_{n,n'}^m$) is a function of the spherical harmonics and hence varies slightly from that of Gumerov. $M|L_{n,n'}^m = M|L_{n,n'}^{m,m}(k, \mathbf{x}_c, \mathbf{y}_c)$. The reduction of the complexity to $O(p^3)$ is thus achieved and the new translation can be expressed as

$$L_n^m(k, \mathbf{x}_c) = M|L_{n,n'}^m(k, \mathbf{x}_c, \mathbf{y}_c) M_{n'}^m(k, \mathbf{y}_c). \quad (24)$$

The co-ordinate system is rotated once to obtain the correct orientation of the vector $\mathbf{x}_c - \mathbf{y}_c$. The complexity of rotating the multipole moments is also $O(p^3)$. The translation requires $O(p^3)$ complexity. Rotating the local expansions back to the original co-ordinate system requires another $O(p^3)$ complexity. Even for the rotations, recursive formulas are used to expedite the process. The rotation of the multipole moments to a new co-ordinate system is dependent only on the spherical harmonics. The detailed formulae for the same are available in the Ref. [23]. As all the operations are $O(p^3)$, the resultant formulation is now $O(p^3)$.

This $O(p^3)$ formulation that is adequate for both low and high frequency applications has been implemented to further improve the efficiencies of the adaptive FMBEM, especially for higher frequency problems. This $O(p^3)$ formulation does not use the Wigner-3j symbol explicitly, which can also reduce the memory usage.

3. FMBEM algorithm for half-space acoustic problems

With all the formulas introduced in Section 2, we are able to construct the 3-D FMBEM algorithm for half-space acoustic wave problems. The adaptive FMM algorithm is described in the following subsections. It is a modified version of the adaptive algorithm reported in Refs. [10,15] for full-space problems.

The FMBEM uses iterative solvers such as the generalized minimum residue method (GMRES) in which the FMM is used to accelerate the multiplication of matrix \mathbf{A} and vector λ (Eq. (6)). The adaptive FMM algorithm consists of the following three steps (A, B, C):

A. *Initialization*: First, an adaptive hierarchical tree of boxes is constructed by dividing the real problem domain (boundary of

the structure) into smaller and smaller sub-domains until the number of elements contained in each leaf (childless box) is less than the maximum number allowed in the box.

B. *Upward pass*: Starting from the lowest level, the multipole moments are calculated for each box (Eqs. (11) and (12)) and translated to the box's parent's center using M2M (Eq. (13)). Continue the M2M until tree level 2 is reached. After the upward pass, every box down from level 2 should have a multipole moment set. The upward pass is exactly the same as the one reported in Refs. [10,15] for full-space FMBEM.

C. *Downward pass*: Starting from level 2 to the lowest level, at each level l , perform the following steps:

Step I: The multipole moments of each box b at level l are M2L (Eqs. (15) and (16)) translated to the local expansions at the center of box c and its mirror box c' , respectively where box c is each box in the interaction list of box b .

After step I, one set of local expansion coefficients is calculated for each box b on level l and another set of local expansion coefficients is obtained for each mirror box b' . Since mirror box center can be determined by the real box center, we associate the mirror box local expansion with its corresponding box in the real domain and refer these two local expansions as the real local expansion and image local expansion of box b .

Step II: If b is not on level 2, use L2L (Eq. (16)) to translate b 's parent box's real local expansion and image local expansion coefficients to box b .

Step III: For box b at the level l which is a leaf box or at the lowest level, calculate $g_{ij}q_j$ and $f_{ij}\phi_j$ for each element i in b using local expansion (Eq. (17)), and adding direct evaluation results (Eq. (5)) for element i in box b and elements j in neighboring leaves of b . (A box is said to be a neighbor of b if it shares at least a boundary point with b .)

Contributions from the following boxes are added using either direct evaluation (Eq. (5)) or M2L translation (Eqs. (15) and (16)) based on the relative complexity and satisfaction of the distance criterion for M2L translation.

1. level l' ($l' > l+1$) leaves that are separated from b (if b is a leaf) by a level l' box.
2. level l' ($l' < l-1$) leaves that are separated from b by a level l' box.

After the downward pass, the vectors $g_{ij}q_j$ and $f_{ij}\phi_j$ are calculated in the current iteration step for the matrix-vector multiplication.

4. Numerical examples

The adaptive half-space FMBEM has been implemented in a code using Fortran 90, which can be applied to solve half-space acoustic wave problems with models of the structures sitting either on or above the infinite and rigid half-space plane.

In all the examples presented below constant triangular elements are used. For the FMM, a maximum number of 100 elements are allowed in a leaf. The GMRES solver will stop the iteration when the residue (relative error) is below the tolerance of 10^{-5} . All the computations for the first two examples presented below were done on a desktop PC with an Intel® 3.0GHz Pentium® IV CPU and 1 GB RAM. For the third example with the windmills, the model was solved on a desktop PC with a 64-bit Intel® Core™2 Duo CPU and 8 GB RAM.

4.1. Sphere models

We choose a sphere with radius $a = 1$ m and $k = 0.5 \text{ m}^{-1}$ as our first model to verify the adaptive half-space FMBEM. The x - y plane is chosen as the infinite rigid plane. Both radiation and scattering problems are considered. The maximum number of multipole and local expansion terms is set to 6 in this example.

We first test the half-space radiation problem. The total number of elements on one sphere is 10,800. The adaptive half-space FMBEM is compared with the full-space FMBEM, in which another identical sphere with the same boundary condition is positioned in the image space symmetrical to the x - y plane. The distance d between the center of the sphere and the rigid plane varies from 0 to 10 m. The case when $d = 0$ indicates that the sphere is cut into two parts by the x - y plane. Only the top hemisphere is modeled in this case using one half of the total number of elements (with 5400 elements) for the half-space FMBEM.

Comparisons of the half-space and full-space FMBEM results are shown in Table 1, in which $|P|$ is the amplitude of the sound pressure on the half plane at a sample point located at (5 m, 0, 0). The boundary condition on the sphere is the Neumann boundary condition with the value given by (0.0, -207.515). The analytical result is available for the first case when $d = 0$, that is, $|P| = 37.1214$. The numbers of iterations required are 4–7 iterations. This table shows very good agreement in the accuracy for both the half-space and full-space results. However,

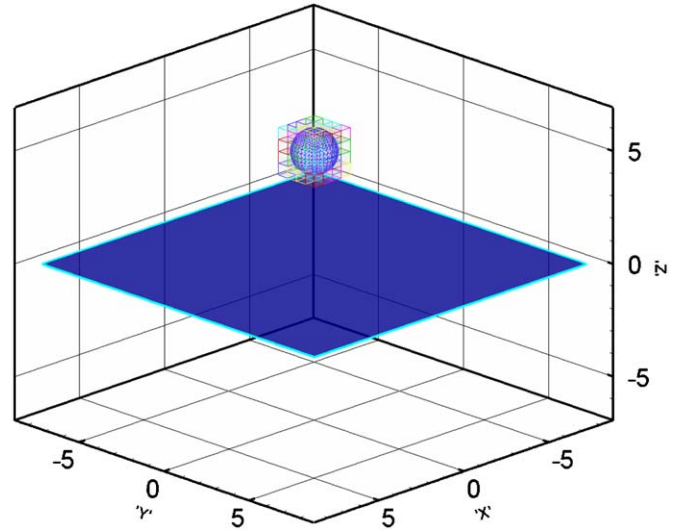


Fig. 3. Half-space FMBEM tree structure for the half-space problem.

the total CPU times for the half-space models are much less than the total CPU time used with the full-space models. This is because the full-space FMBEM needs an extra sphere in the image domain and the size of the tree structure increases substantially as the distance between the sphere and the rigid plane increases, as shown in Figs. 2 and 3. Figs. 4 and 5 show the contour plots of the pressures computed using the full-space FMBEM and half-space FMBEM on the half-space model, respectively, when the distance $d = 4$ m.

Table 1 Results for the radiating sphere model (with 10,800 elements per sphere).

Distance d	Half-space FMBEM		Full-space FMBEM	
	$ P $	CPU (s)	$ P $	CPU (s)
0	37.0856 ^a	98.09	37.1061 ^a	121.64
1	71.8088	82.92	71.8120	106.30
2	70.2521	83.03	70.2517	122.56
5	52.0601	83.08	52.0589	110.91
10	33.3989	83.25	33.3992	98.25

^a Note: The analytical solution in this case ($d = 0$) is 37.1214.

Next, we study the convergence and stability of the half-space FMBEM code using the radiation problem with the total number of elements ranging from 300 to 97,200 for the case $d = 3$ m. The number of iterations required is 4. The convergence plots for both the half-space FMBEM and the full-space FMBEM are presented in Fig. 6, which shows that the sound pressure at the sample point at (0, 0, 0) converges very quickly for both the approaches and the numerical results are very stable for large numbers of the elements on a single sphere. As shown in Fig. 7, the half-space FMBEM uses much less total CPU times than the full-space FMBEM, especially for larger models where the additional overhead used for the half-space FMBEM is relatively small.

Finally, we test a half-space scattering problem using the same sphere model where the sphere is sitting at the distance $d = 2$ m and impinged upon by a plane incident wave traveling in the $+x$ direction. The incident wave has a unit amplitude and the non-dimensional wavenumber $ka = 1$. The sphere is meshed with 10,800 elements. The contour plot of the pressure computed using the half-space FMBEM is shown in Fig. 8, where the pressure values on the sphere match with those obtained by using the corresponding full-space FMBEM. Again, the total CPU time for the half-space FMBEM is about one half of the CPU time used for the equivalent full-space model.

4.2. Sound barrier models

After verifying the accuracy and efficiency of the half-space FMBEM on the sphere models, we examine the influence of a sound barrier placed between a point source and a rigid building using the half-space FMBEM. Much research on the 2-D simulation of the acoustic barriers has been conducted. However, 2-D simulation is based on the assumption that the barrier and the

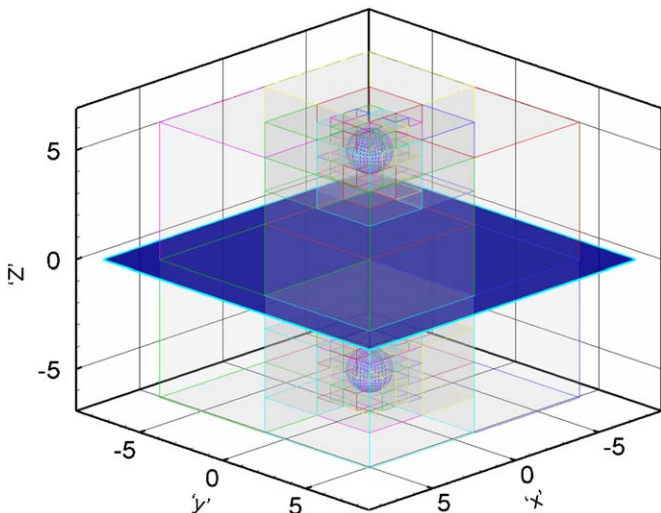


Fig. 2. Full-space FMBEM tree structure for the half-space problem.

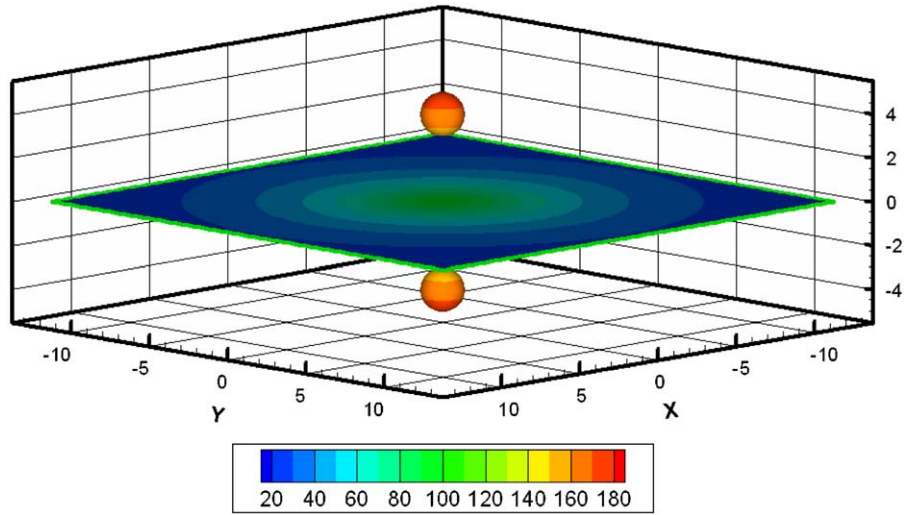


Fig. 4. Plot of sound pressure on the radiating sphere using the full-space FMBEM.

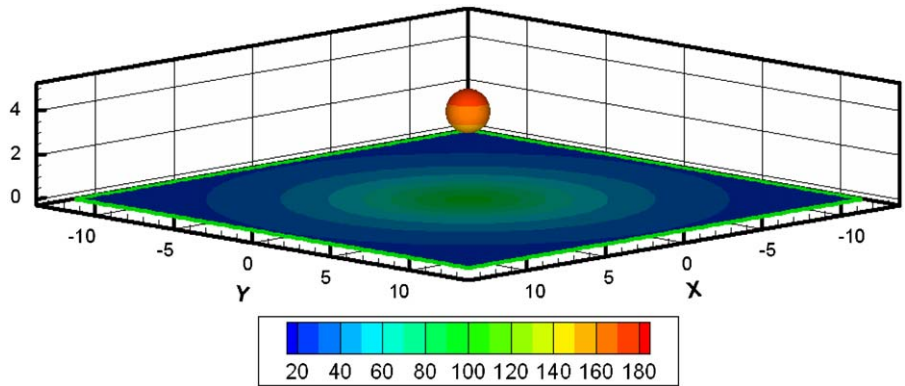


Fig. 5. Plot of sound pressure on the radiating sphere using the half-space FMBEM.

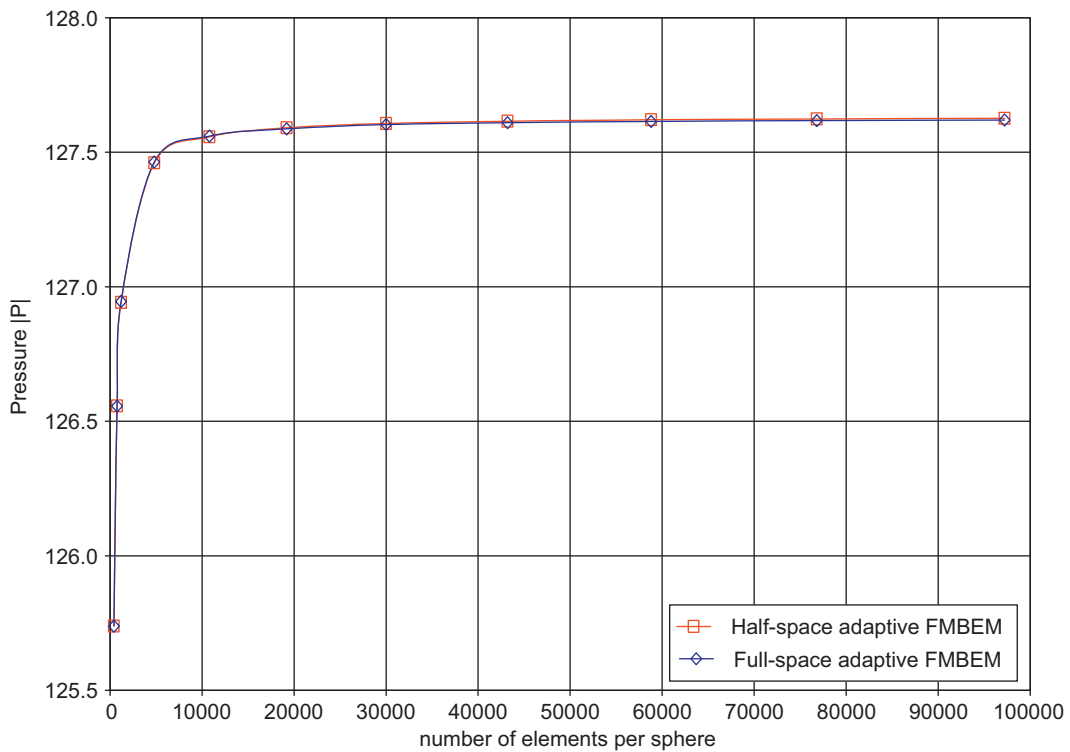


Fig. 6. Convergence comparison between the half-space and full-space FMBEM.

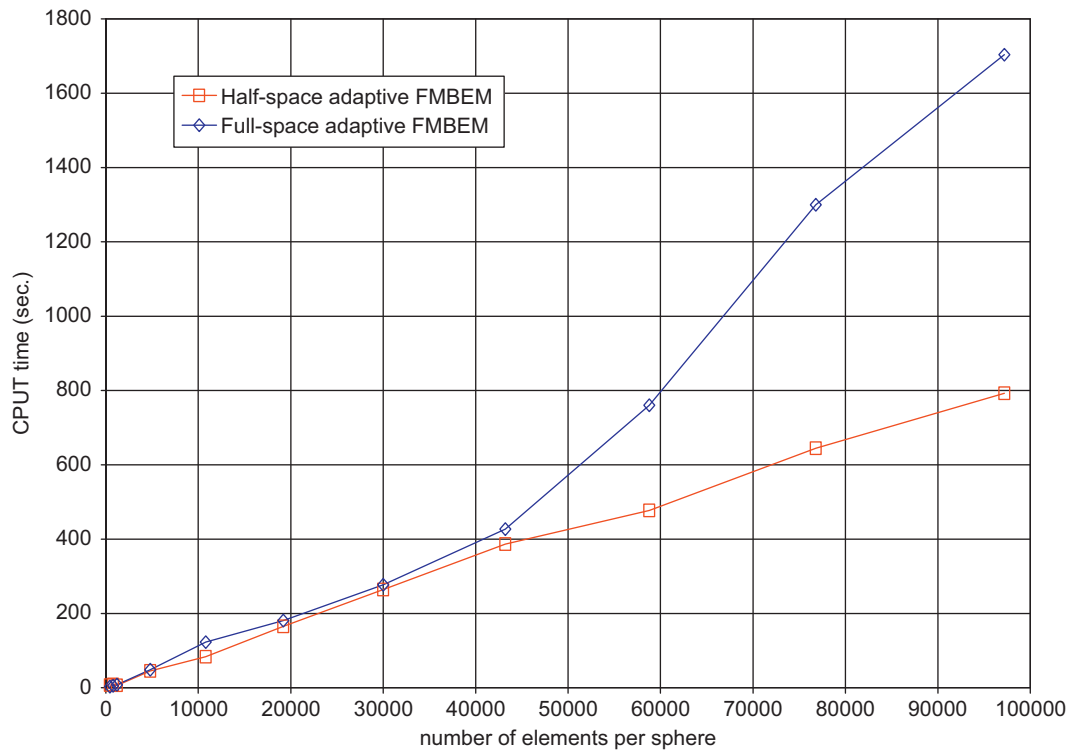


Fig. 7. CPU time comparison between the full-space and half-space FMBEM.

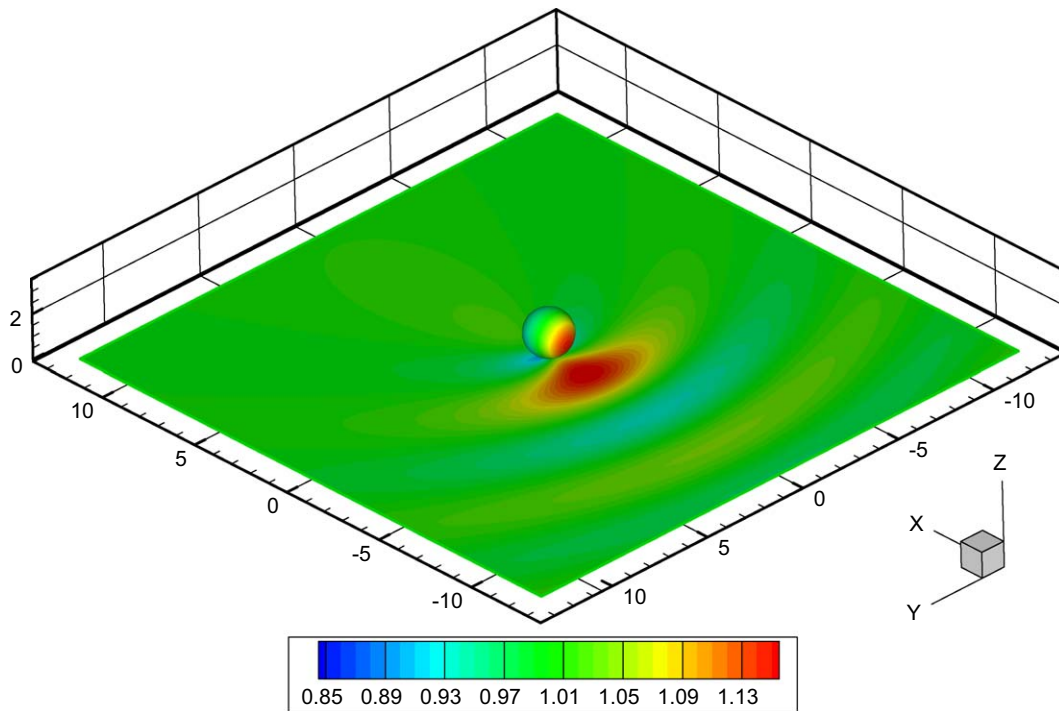


Fig. 8. Scattering from the sphere in the half space (total sound pressure field plotted).

structure are straight and infinitely long, which may not be accurate. Due to the high computing cost with the conventional BEM, the 3-D BEM can only simulate a sound barrier with very short length. With the FMBEM, long and curved barrier can be modeled.

In the first sound barrier example, the ground surface, barrier and building are modeled as non-absorbing rigid surfaces. An acoustic point source of 1 Pa (corresponding to a sound pressure level (SPL) of about 94 dB) is placed 50.0 m away from a building and 1 m above the ground, with $k = 0.5 \text{ m}^{-1}$. A quarter-circular

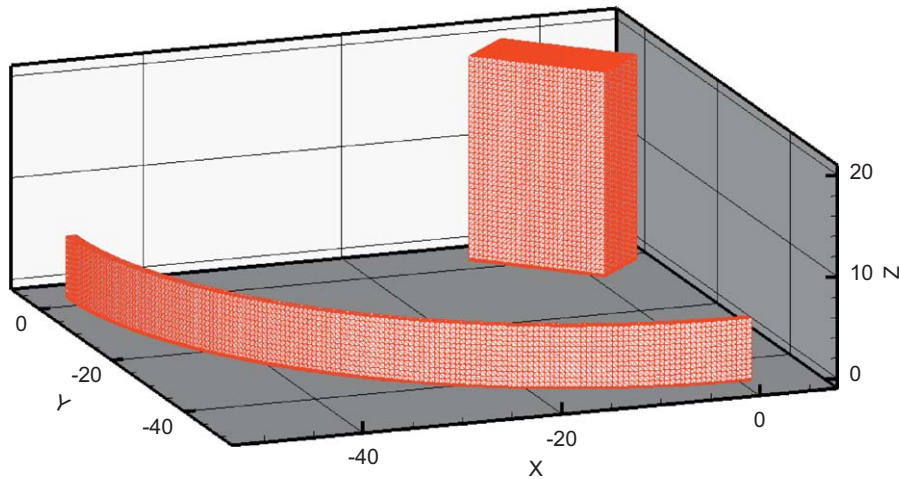


Fig. 9. Half-space sound barrier model (3-D view).

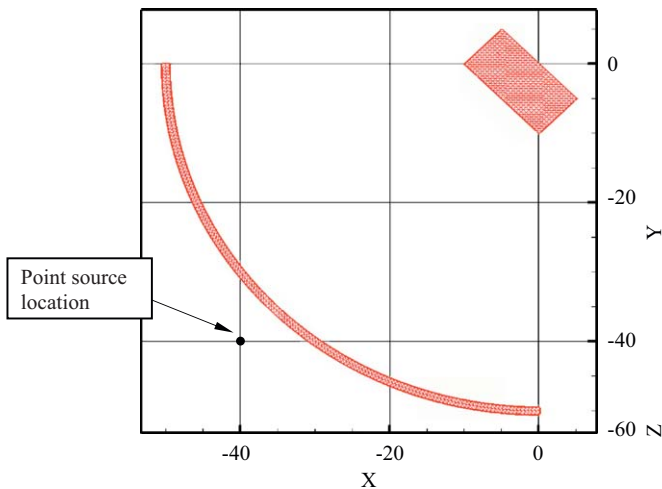


Fig. 10. Half-space sound barrier model (2-D view).

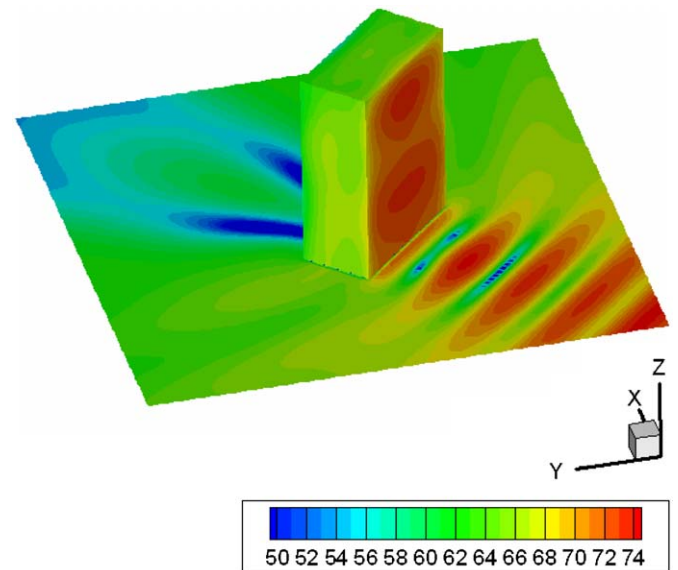


Fig. 11. Contour plot of sound pressure level (dB) on the building without a barrier.

barrier of radius $R = 50$ m and initial height $h = 2$ m is inserted between the source and the building to reduce the acoustic sound registered on the building. The closest distance between the source and barrier is 7 m. The barrier is modeled as a 1-m-thick body. The boundary elements used to discretize the building and barrier has a size of 0.5 m. Figs. 9 and 10 show the dimensions of the model and the BEM mesh with triangle elements. The wavenumber $k = 0.5$ is used for this representative analysis. The resultant frequency is about 28 Hz. The ka value for these problems is relatively high (ka is about 35). The maximum number of multipole and local expansion terms is set to 20 to get better accuracy for solving these problems.

Fig. 11 gives the sound pressure level in decibel when no barrier is present. Fig. 12 shows the contour plot of the dB on the building and 2-m-high barrier, when the 2-m-high barrier between the source and the building is placed. The contour plot indicates poor performance of this low barrier. However, after increasing the height of the barrier from 2 to 4 m and then to 6 m, there are marked decreases in the sound pressure levels, as shown in Figs. 13 and 14.

The results and performance of the half-space FMBEM in simulations of the sound barrier and building are summarized in Table 2. The numbers of iterations required are 23–39. It is shown that the half-space FMBEM is efficient and able to handle these practical problems.

4.3. Wind turbine model

The analysis of the windmill noise is presented as the last example to illustrate the potential usefulness of the half-space acoustic FMBEM code for modeling large-scale half-space acoustic problems. The blades of the windmill considered are 10 m long and the total height of the windmill is 28.68 m. Each windmill is discretized using 111,494 boundary elements. A total of five windmills are considered for the analysis with a total number of 557,470 elements. The windmills are placed 50 m

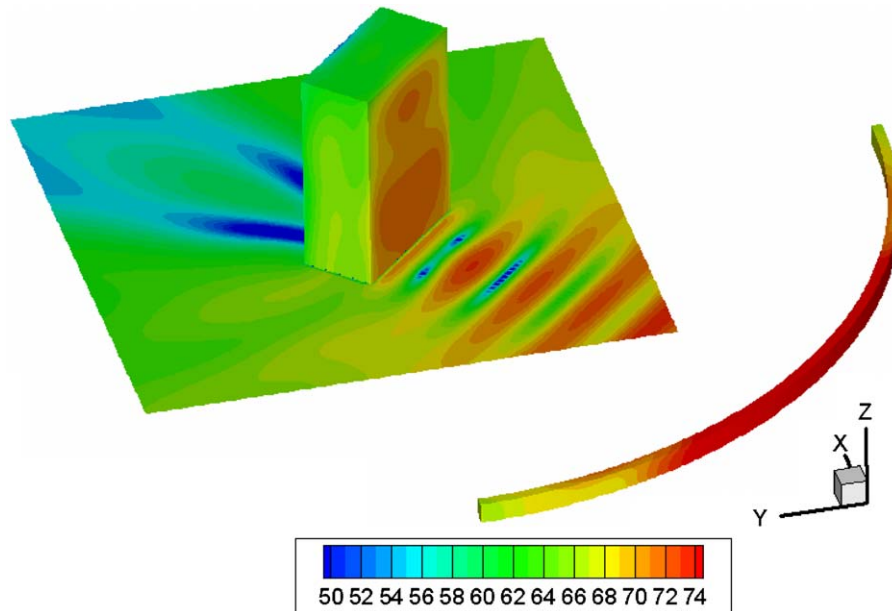


Fig. 12. Contour plot of SPL (dB) for a 2 m high barrier and the building.

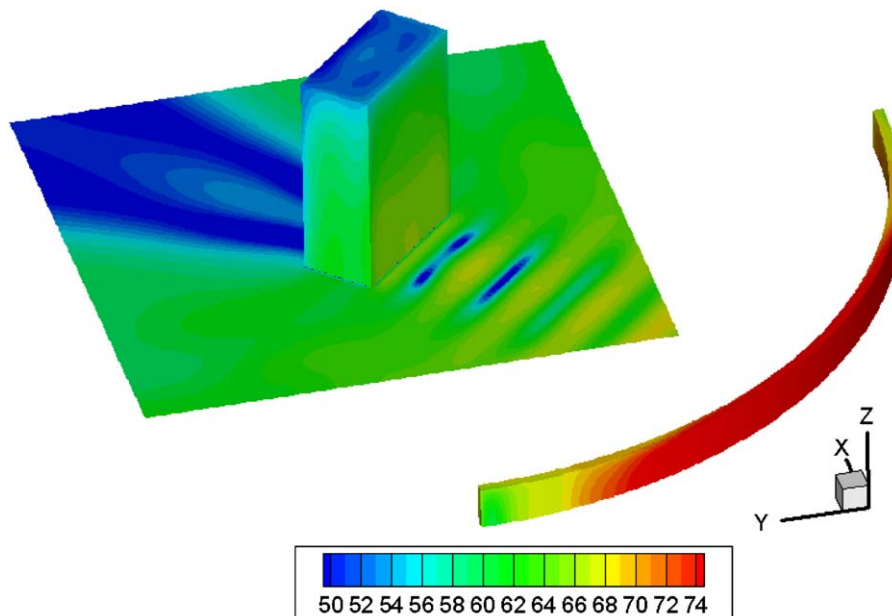


Fig. 13. Contour plot of SPL (dB) for a 4 m high barrier and the building.

apart in the x and y directions. A velocity boundary condition calculated using a rotation of the blades are applied to all the blades of the windmill and zero velocity condition elsewhere. The wavenumber $k = 0.05 \text{ m}^{-1}$ is used for this analysis. The maximum number of multipole and local expansion terms was set to 10 for this problem.

The solution for the entire windmill BEM model took about 3778 s on a 64-bit Intel® Core™2 Duo desktop PC with 8 GB RAM. The number of iterations required is 13. The sound pressure level was calculated first for the boundaries of the windmills (Fig. 15)

and then on a $200 \text{ m} \times 200 \text{ m}$ field surface (on the x - y plane) composed of 10,201 field points (Fig. 16). The time used in calculating the field values (one matrix-vector multiplication) is 300 s using the FMM and 1200 s using the conventional direct method.

This analysis of the windmills is preliminary, aimed only to show the potential of the FMBEM for modeling such large-scale half-space acoustic problems. Further studies of the windmill noise problems can be conducted with more realistic conditions.

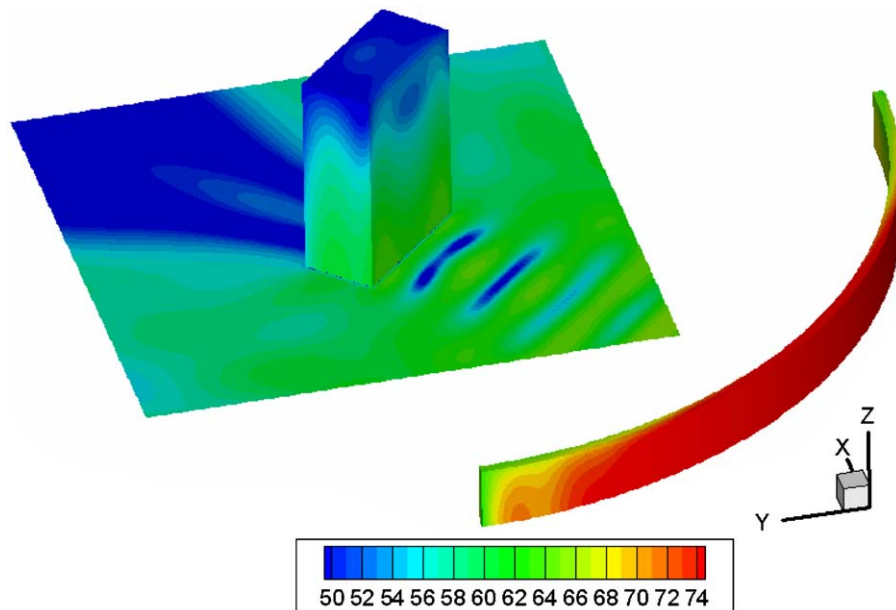


Fig. 14. Contour plot of SPL (dB) for a 6 m high barrier and the building.

Table 2
Results for the acoustic barrier analysis.

	Number of elements	Max dB on building	CPU time (s)
Building without barrier	7910	73.61	562
Building with 2 m high barrier	11,122	71.84	1230
Building with 4 m high barrier	13,698	66.03	1711
Building with 6 m high barrier	16,274	63.88	1966

5. Discussions

An adaptive BEM is presented in this paper for modeling 3-D half-space acoustic wave problems. Instead of using the mirror image technique to the discretized BEM systems of equations for half-space acoustic problems, the half-space Green's function is adopted in the BIE formulation explicitly, which ensures that the hierarchical tree structure in the FMBEM can be constructed in the real domain only. The adaptive algorithm is also used in the half-space FMBEM, thus, the memory usage and CPU time are significantly less than the full-space FMBEM. The accuracy of the half-space FMBEM is found to be comparable to that of the full-space FMBEM.

More improvements can be made for the adaptive FMBEM for modeling half-space problems. Diagonal translation that was proposed by Rokhlin [20] and Lu and Chew [24] can be used to speed up the half-space FMBEM in even higher frequency ranges. Wideband fast multipole formulation [21] can also be considered that can seamlessly integrate the low and high frequency approaches. Although it is easy to implement in the code to use the tree structure only for the real boundary of the object, it might be beneficial to use a tree structure that covers both the real and

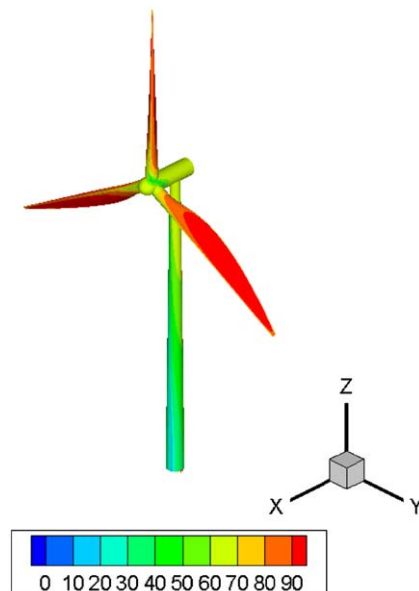


Fig. 15. Plot of sound pressure level (dB) on a single windmill.

image boundaries. In this way, the M2L translations from the expansion points to the image points may be more efficient due to the larger distance. This approach can be explored in the future work.

The applicability of the developed adaptive half-space FMBEM discussed in this paper is, however, not limited to acoustic problems. This adaptive half-space algorithm can also be extended to solve many other half-space problems, such as potential, electrostatic, electromagnetic and other problems using the fast multipole BEM.

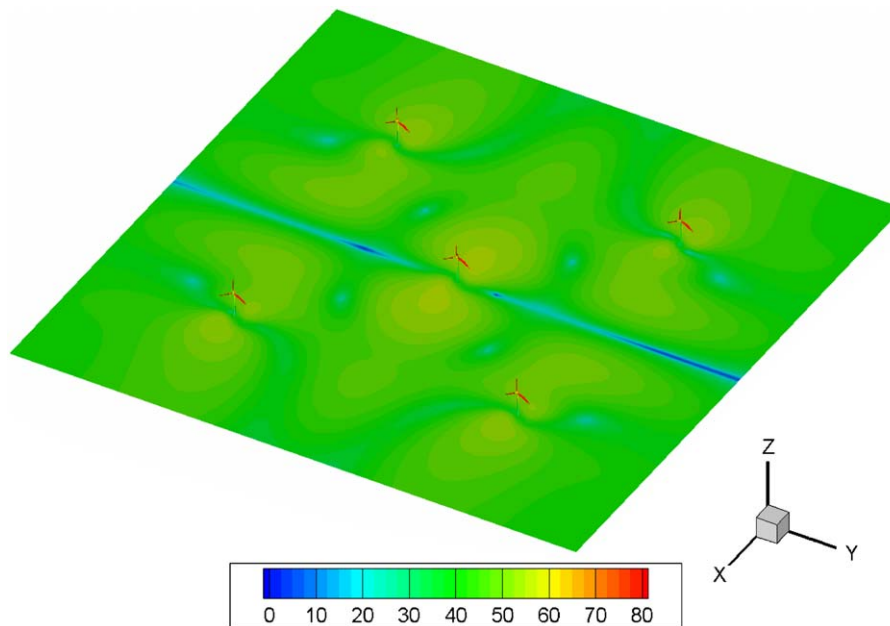


Fig. 16. Plot of the SPL (dB) on the field surface and five windmills (DOFs = 557470).

Acknowledgement

The authors would like to thank Mr. Bo Bi for creating the CAD model of the windmill used in this study.

References

- [1] Seybert AF, Soenarko B. Radiation and scattering of acoustic waves from bodies of arbitrary shape in a three-dimensional half space. *ASME Trans J Vib Acoust Stress Reliab Des* 1988;110:112–7.
- [2] Rokhlin V. A fast algorithm for the discrete Laplace transformation. *J Complexity* 1988;4(1):12–32.
- [3] Greengard L, Rokhlin V. A fast algorithm for particle simulations. *J Comput Phys* 1987;73:325–48.
- [4] Engheta N, Murphy WD, Rokhlin V, Vassiliou MS. The fast multipole method (FMM) for electromagnetic scattering problems. *IEEE Trans Ant Propag* 1992;40(6):634–41.
- [5] Chen YH, Chew WC, Zeroug S. Fast multipole method as an efficient solver for 2D elastic wave surface integral equations. *Comput Mech* 1997;20(6):495–506.
- [6] Song J, Lu C-C, Chew WC. Multilevel fast multipole algorithm for electromagnetic scattering by large complex objects. *IEEE Trans Ant Propag* 1997;45(10):1488–93.
- [7] Koc S, Chew WC. Calculation of acoustical scattering from a cluster of scatterers. *J Acoust Soc Am* 1998;103(2):721–34.
- [8] Fischer M, Gauger U, Gaul L. A multipole Galerkin boundary element method for acoustics. *Eng Anal Boundary Elem* 2004;28(2):155–62.
- [9] Darve E, Havé P. Efficient fast multipole method for low-frequency scattering. *J Comput Phys* 2004;197(1):341–63.
- [10] Shen L, Liu YJ. An adaptive fast multipole boundary element method for three-dimensional acoustic wave problems based on the Burton–Miller formulation. *Comput Mech* 2007;40(3):461–72.
- [11] Nishimura N. Fast multipole accelerated boundary integral equation methods. *Appl Mech Rev* 2002;55(4 (July)):299–324.
- [12] Liu YJ. *Fast multipole boundary element method-theory and applications in engineering*. Cambridge: Cambridge University Press; 2009.
- [13] Yasuda Y, Sakuma T. A technique for plane-symmetric sound field analysis in the fast multipole boundary element method. *J Comput Acoust* 2005;13(1):71–85.
- [14] Cheng H, Greengard L, Rokhlin V. A fast adaptive multipole algorithm in three dimensions. *J Comput Phys* 1999;155:468–98.
- [15] Shen L, Liu YJ. An adaptive fast multipole boundary element method for three-dimensional potential problems. *Comput Mech* 2007;39(6):681–91.
- [16] Yoshida K. *Applications of Fast Multipole Method to Boundary Integral Equation Method*, in Department of Global Environment Engineering. 2001, Kyoto University: Kyoto, Japan.
- [17] Gumerov NA, Duraiswami R. *Fast, Exact, and Stable Computation of Multipole Translation and Rotation Coefficients for the 3-D Helmholtz Equation*. 2001, UMIACS Technical Report TR 2001-44, University of Maryland, Institute for Advanced Computer Studies, College Park, MD.
- [18] Chew WC. Recurrence relations for three-dimensional scalar and addition theorem. *J Electromagn Waves Appl* 1992;6:133–42.
- [19] Ong ET, Lee HP, Lim KM. A fast Fourier transform on multipoles (FFTM) algorithm for solving Helmholtz equation in acoustics analysis. *J Acoust Soc Am* 2004;116(3):1362–71.
- [20] Rokhlin V. Diagonal forms of translation operators for the Helmholtz equation in three dimensions. *Appl Comput Harmon Anal* 1993;1(1):82–93.
- [21] Cheng H, Crutchfield WY, Gimbutas Z, Greengard LF, Ethridge JF, Huang J, et al. A wideband fast multipole method for the Helmholtz equation in three dimensions. *J Comput Phys* 2006;216(1):300–25.
- [22] Gumerov NA, Duraiswami R. Recursions for the computation of multipole translation and rotation coefficients for the 3-D Helmholtz equation. *SIAM J Sci Comput* 2003;25(4):1344–81.
- [23] Gumerov NA, Duraiswami R. *Fast multipole methods for the Helmholtz equation in three dimensions*. Amsterdam: Elsevier; 2004.
- [24] Lu C, Chew W. Fast algorithm for solving hybrid integral equations. *IEE Proc-H* 1993;140(6):455–60.